Journal of Hazardous Materials 386 (2020) 121947

Contents lists available at ScienceDirect

Journal of Hazardous Materials

journal homepage: www.elsevier.com/locate/jhazmat

Distorted polymeric carbon nitride via carriers transfer bridges with superior photocatalytic activity for organic pollutants oxidation and hydrogen production under visible light

Chengyun Zhou, Guangming Zeng*, Danlian Huang*, Yuan Luo, Min Cheng, Yang Liu, Weiping Xiong, Yang Yang, Biao Song, Wenjun Wang, Binbin Shao, Zhihao Li

College of Environmental Science and Engineering, Hunan University and Key Laboratory of Environmental Biology and Pollution Control (Hunan University), Ministry of Education, Changsha 410082, PR China

GRAPHICAL ABSTRACT

ARTICLE INFO

Editor: Danmeng Shuai

Keywords:
Polymeric carbon nitride
2,5-dibromopyrazine
Carrier channel
Photocatalytic H_2 evolution
Sulfamethazine degradation

ABSTRACT

Polymeric carbon nitride (PCN) has become the most promising metal-free photocatalysts but its activity is low. Molecule doping of PCN has been proved to be an effective strategy to achieve high photocatalytic performance. Herein, we report a bottom-up method to synthesize modified PCN, which includes 2,5-dibromopyrazine doping, thermal-induced exfoliation and condensation/polymerization. The incorporation of electron-deficiency 2,5-dibromopyrazine into the PCN framework can effectively tune the electronic structures and improve the charge-carrier separation. In addition, the incorporation of 2,5-dibromopyrazine induced significant structural changes from planar symmetric to distortion. The optimized pyrazine doped PCN showed a reaction rate enhancement of 4-fold for the degradation of sulfamethazine compared to that of conventional urea-based PCN. Further reactive species and degradation intermediate detection studies, indicated that $^{\cdot}O_2^-$ was generated during the photocatalytic process, which could lead to the decomposition, and finally mineralization of sulfamethazine. 2,5-Dibromopyrazine doped PCN also leads to a 6.3-fold improvement in H_2 generation with the visible light. Especially, phytotoxicity experiments showed that the toxicity of sulfamethazine after degradation is greatly reduced, and the as-prepared photocatalyst is environmentally friendly.

* Corresponding author at: College of Environmental Science and Engineering, Hunan University, Changsha, Hunan 410082, PR China.
E-mail addresses: zgming@hnu.edu.cn (G. Zeng), huangdanlian@hnu.edu.cn (D. Huang).

https://doi.org/10.1016/j.jhazmat.2019.121947
Received 12 November 2019; Received in revised form 15 December 2019; Accepted 20 December 2019
Available online 21 December 2019
0304-3894/

1. Introduction

In recent years, micro-pollutants (i.e. antibiotics and endocrine disrupting chemicals) in aquatic environments have attracted increasing concerns (Bolong et al., 2009; Ye et al., 2017). Sulfamethazine (SMZ) is a typical sulfonamide antibiotic that is intensively used in medicine, aquaculture, livestock and poultry farming (Shimizu et al., 2013; Chen et al., 2017). Studies indicated that about 30 %–90 % of sulfonamides drugs or its metabolites are released through urine and excrement into the surface and subsurface water bodies, which can become a potential risk to human health (Gong et al., 2009; Xu et al., 2012). Photocatalytic water treatment as a green and sustainable advanced oxidation process has great potential in removing organic pollutants from wastewater (Ong et al., 2016; Sprick et al., 2015; Song et al., 2019; Huang et al., 2019a). On the other hand, photocatalytic water splitting has been regarded as a sustainable way to solve the energy crisis (Zhang et al., 2019; Xia et al., 2019). Therefore, it is urgent to explore effective and stable photocatalyst for hydrogen evolution reaction and water purification. In the past decades, many semiconductor materials, such as TiO_2, CdS, Bi_2WO_6, $Bi_{12}O_{17}Cl_2$ and polymeric carbon nitride (PCN), have been explored for photocatalytic reactions under UV and visible light irradiation (Zhou et al., 2018a, b; Linsebigler et al., 1995; Utterback et al., 2016; He et al., 2018; Ye et al., 2019; Huang et al., 2019b).

Among these novel photocatalysts, PCN has attracted much attention due to the suitable band structure and the appropriate optical absorption (Wang et al., 2019a; Yang et al., 2019; Huang et al., 2019c; Zheng et al., 2018; Yang et al., 2017; Xu et al., 2017). It also exhibits excellent chemical stability. PCN has been extended studied in photocatalytic degradation, water splitting and inactivation of microorganism due to its low cost and nontoxicity characters (Wang et al., 2019b; Huang et al., 2018; Ming et al., 2019; Zheng et al., 2015; Xu et al., 2014). However, PCN as a typical polymer, the local structure was rather disordered and the exciton binding energy was high, leading to the insufficient separation of charge carriers. Moreover, the light adsorption edge of pristine PCN is below 460 nm. So, the photocatalytic application of PCN has been limited by these above demerits (Li et al., 2020; Duan et al., 2019). Enormous efforts have been explored to improve the photocatalytic activity of PCN, which including element doping, coupling with other semiconductors, and molecular doping copolymerization (Zhou et al., 2018c; Xing et al., 2018; Zhou et al., 2019a; Cheng et al., 2019a; Wu et al., 2019; Cheng et al., 2018). Especially, molecular copolymerization is a unique and effective method that can modify the structure and properties by introducing organic molecules into the PCN framework.

Recently, copolymerizing similar aromatic structure with PCN precursors has been a typical molecular assembly method to extend the π electrons of the PCN aromatic system and modulate the electronic band structure, leading to affect its photocatalytic activity (Zhou et al., 2018d, b; Yu et al., 2017; Jiang et al., 2019). Some organic molecules have been employed to dope into PCN like benzene-based molecules, thiophene-based molecules and nitric heterocyclic-based molecules and many more (Zhou et al., 2018e; Yu et al., 2018; Dong et al., 2019; Wen et al., 2019; Zhang and Wang, 2014). Yan et al. developed aromatic ring substituting doping PCN by using urea and 2, 4, 6-trichlorophenol as the precursors (Yan et al., 2018). The hydrogen evolution rate (HER) of modified PCN reached as high as 12.543 mmol h^{-1} g^{-1}, which is higher than that of pristine CN (1.071 mmol h^{-1} g^{-1}). Li et al. prepared pyrimidine-doped PCN by using urea and 2, 4-diaminopyrimidine as comonomers (Li et al., 2019). The extended light adsorption and the enhanced charge transport of pyrimidine-doped PCN resulted in the enhancement of HER activity (from 0.46 mmol h^{-1} g^{-1} to 2.8 mmol h^{-1} g^{-1}). However, it should be noticed that the research studies focused on limited skeletal structures (i.e. aromatic, pyrimidine) and applied in HER, more heterocyclic structure like pyrazine chemicals should be explored. Pyrazine and its derivatives have been used as acceptor comonomers in donor-acceptor semiconducting polymeric materials. Therefore, it was expected that molecular doping of the PCN framework via integrating pyrazine is a feasible strategy to modify its surface properties and charge carriers transfer, which may leads to the positive effect on photocatalytic reactions.

In this context, urea and 2,5-dibromopyrazine was chosen as the precursors for prepared pyrazine-modified PCN photocatalysts (denoted as PCN-DP). Compared with other precursors, urea-derived PCN has a high degree of polymerization and shows the best photocatalytic performance. The dibromo group in 2,5-dibromopyrazine as the comonomer was able to react with urea and then incorporated into the PCN framework. After incorporating 2,5-dibromopyrazine into the framework of PCN, the PCN-DP sample exhibited enlarged visible light absorption range, suppressed electron-hole recombination rates and promoted charge transfer, which endows them as an excellent candidate for photocatalytic oxidation of organic pollutants and hydrogen evolution. In addition, the phytotoxicity of the wastewater (before and after photocatalytic treatment) and photocatalysts were evaluated to illustrate the toxicity of the degradation products and photocatalysts to the plants as this relates to the reuse of water.

2. Experimental section

2.1. Catalysts preparation

The typical bulk carbon nitride was obtained by a traditional polymerization as reported previously (Zhou et al., 2019a). Typically, 10 g of urea (99 %, AR) were added into a ceramic crucible with a cover and heated to 550 °C with a heating rate of 5 °C min^{-1} and kept for 2 h in air condition. The obtained product was then further heated to 550 °C for another 2 h with a ramp rate of 10 °C min^{-1}. After cooling to room temperature, the obtained product was washed with distilled water. The yellow powders was further dried at 70 °C and denoted as PCN.

The PCN-DP samples were prepared from bottom-up method by thermal-induced exfoliation and polymerization. Typically, 10.0 g of urea and a series of 2, 5-dibromopyrazine (0.1 g, 0.2 g, and 0.4 g) were fine mixed in 3 mL ethanol by ball milling. The obtained mixed precursors were put into a ceramic crucible with a cover and heated to 550 °C with a heating rate of 5 °C min^{-1} and kept for 2 h in air. The obtained product was then further heated to 550 °C for another 2 h with a ramp rate of 10 °C min^{-1}. The final product was dried at 70 °C after water wash and denoted as PCN-DP-x, where x indicates the amount of DP (x = 0.1 g, 0.2 g, and 0.4 g).

2.2. Characterization

The crystal phase of samples were investigated by Rigaku D/max-2500 X-ray diffraction (XRD) with Cu *Kα* radiation (λ = 0.15406 nm). The morphology of samples was collected by scanning electron microscopy (SEM, FEI Helios NanoLab 600i) and transmission electron microscopy (TEM, FEI tecnai G2F20 electron microscope). Fourier transform infrared spectroscopy (FTIR) spectra were measured on BIORad FTS 600 spectrometer in the range of 500-4000 cm^{-1}. The chemical states were obtained at X-ray photoelectron spectra (XPS, ESCALAB 250Xi). The light absorption was analyzed on UV–vis diffuse reflectance spectra (DRS, Cary 300). Steady room temperature photoluminescence (PL) spectra were conducted in a Perkin Elmer luminescence spectrometer (LS 50 B) with the excitation wavelength of 365 nm. The electron paramagnetic resonance (EPR) of solid and liquid samples was performed on Bruker ER200-SRC spectrometer.

2.3. Photocatalytic performance evaluation

The photocatalytic system was set up in a photochemical reactor under visible light irradiation. The model pollutant used was

sulfamethazine (SMZ) (Zhang et al., 2018). A typical sequence test contained 25 mg catalyst and 10 mg L^{-1} SMZ in 50 mL of water solution. The mixed solution was stirred without light for 1 h to obtained the adsorption and desorption equilibrium. Then, the reactor was irradiated by a 300 W Xenon lamp with a 420 nm cutoff filter. 1 mL suspension was extracted from the reactor in every 15 min and centrifuged at a certain amount of time. The concentration of SMZ was detected by high-performance liquid chromatography (HPLC, Agilent 1260 infinity) with the C_{18} column (4.6 × 150 mm). The HPLC analysis was carried out using an eluent of water and acetonitrile (65:35, v/v) for SMZ. The flow rate of eluent was 1 mL min^{-1} and the detection wavelength was set as 265 nm. The analysis of degradation products was detected by high-performance liquid chromatography- mass spectra (HPLC-MS) and the method was listed in Text S1. In addition, the photocatalytic hydrogen evolution tests were detailed in Text S2.

2.4. Photoelectrochemical measurement

The PCN and PCN-DP electrodes were prepared by drop-coating method. 3 mg of catalyst was dispersed in 1 mL of 0.5 % Nafion-ethanol solution, and then the solution was under sonication for 2 h. The obtained mixture was dropped onto the clean F-doped tin oxide (FTO) glass with an effective area of 1 cm × 1 cm. The electrode was then put into muffle furnace for 2 h calcination at 130 ˚C. After cooling to room temperature, the working electrodes, the Pt plate electrode (40 × 0.55 mm, 99 %), and the Ag/AgCl electrode were immersed in 0.2 M Na_2SO_4 aqueous solution in a three-electrode cell. The test was performed on a CHI 660D workstation. The visible light was offered by a 300 W xenon lamp with a 420 nm cutoff filter. The photocurrent responses of the samples upon light on and off were measured. Electrochemical impedance spectroscopy (EIS) was performed in 100 mL of 0.2 M Na_2SO_4 aqueous solution with 0 V of applied voltage. A Mott-Schottky plot was obtained at a frequency of 900 and 1000 Hz.

2.5. Phytotoxicity test

The phytotoxicity of samples was determined by seed germination and radicle elongation tests with Chinese cabbage (*Brassica rapa* L.) seeds according to the methods of Luo et al. (Luo et al., 2019). Five samples were tested, which including pure water, SMZ solution (10 mg L^{-1}, before photocatalytic), SMZ solution (10 mg L^{-1}, after photocatalytic), PCN solution (1 g L^{-1}) and PCN-DP-0.2 (1 g L^{-1}), respectively. Pure water was used as the control in the tests. After the surface of seeds being cleaned, 160 individuals were put onto a piece of paper wetted by 5 mL samples in a 90-mm Petri dish for a time. They were kept in an incubator at 25℃ in the dark. After the first incubation stage (24 h), the germinated seeds were recorded to calculate the seed germination rate. And then 20 germinating seeds with similar sizes were selected and then transferred to a new plate containing the same samples for four times. After another 24 h, the radicle length was measured.

3. Results and discussion

3.1. Photocatalyst characterization

Typically, PCN was obtained from urea, while PCN-DP-x was prepared from urea and 2, 5-dibromopyrazine (x represents the mass of 2, 5-dibromopyrazine, ranging from 0.1 to 0.4 g). The XRD patterns of PCN and PCN-DP-x samples are shown in Fig. 1a. The typical XRD peaks at 13.2° and 27.7° corresponding to (100) inter-planar packing of *s*-triazine units and (002) interlayer stacking were obtained for PCN and PCN-DP-x (Xu et al., 2019). Compared with PCN, the intensity of two peaks for PCN-DP was weakened, suggested that the long-range order in atomic arrangements has been destructed by molecular doping and re-calcination (Zhang and Wang, 2013). Moreover, the results of FT-IR (Fig. 1b) further confirmed the molecule doping of pyrazine. The FT-IR bands at 1200 − 1600 cm^{-1}, 810 cm^{-1} can be ascribed to the distinctive aromatic C—N heterocycles and triazine units of PCN (Yu et al., 2017; Li and Zhang, 2018; Liu et al., 2017). High resolution FT-IR was recorded for PCN and PCN-DP samples (Fig. 1c). Among those peaks, typical peak of PCN likes 1510 cm^{-1} gradually towards the longer wavenumber with the increased addition of pyrazine. It could be caused by an interaction between the pyrazine group and the intrinsic structure of PCN (Xiong et al., 2018; Kim et al., 2017).

Organic elemental analysis (OEA) was performed to confirm the introduction of DP in carbon nitride framework (Table S1). It was expected that the C/N atomic ratio would be increased slightly if the DP incorporated successfully. The C/N atomic ratio of PCN-DP-0.2 slightly increased by contrast to PCN (from 0.65 to 0.68). In order to further study the local binding chemical environments of PCN and PCN-DP samples, XPS analyses were carried out. Carbon, nitrogen, and little amounts of oxygen were observed in the spectra of PCN-DP-0.2 (Fig. 1d). Of notice was the absence of bromide characteristics that indicated successful elimination of copolymerization. The C 1s and N 1s of PCN and PCN-DP-0.2 are exhibited in Fig. 1e and f, respectively. The C 1s of samples could be separated into two peaks at 288.3 and 284.7 eV. These peaks were assigned to the N—CN bonds and the CC═— bonds. After pyrazine doping, the percentage of C—C bonds to all carbon increased from 4.0 % (PCN) to 12.6 % (PCN-DP-0.2), which indicated that other carbon source had incorporated into the carbon nitride system (Fan et al., 2015a). On the other hand, the N 1s spectra were fitted into three major peaks at 398.4, 399.8, and 400.9 eV, which correspond to C-N═C for the s-triazine, the tertiary nitrogen, and the C—NH— bonds, respectively (Tong et al., 2017). A slightly increased of C/N atomic percentage from 0.74 for PCN to 0.79 for PCN-DP-0.2 was also identified by XPS (Table S1), indicating that pyrazine ring has been incorporated in PCN framework successfully.

The morphology change of PCN and PCN-DP-0.2 can obtain by SEM and TEM, as shown in Fig. 2. PCN showed a smooth sheet-like morphology (Fig. 2a), while PCN-DP samples exhibited coral-like and hierarchical network structure (Fig. 2b, 2c and 2d). These results show that the incorporation of a small amount of DP could change the morphology of PCN. The distortion structure in PCN-DP samples allow more n-π^* transitions from the edge nitrogen atoms to the conduction band, which might also benefit for the visible photon absorption. In addition, the EDS of PCN-DP-0.2 show the distribution of C and N with trace amount of Br (Fig. S1). The TEM image further indicated the nanosheet-like and pore structural of PCN-DP-0.2. Fig. 2e exhibits that the PCN sample is composed of several thin layers. Fig. 2f and Fig. S2 illustrates that the similar thin layer of PCN-DP-0.2 sample with some irregular pores (the average diameter was 8.9 ± 2.7 nm). The thin layer and porous structure of PCN-DP-0.2 are beneficial to the absorption of light, provide more reactive reaction sites for the reactive species, and improve the photocatalytic activity. N_2 adsorption-desorption measurements further supported the structural changes in PCN-DP materials. Moreover, it was found that all samples matched mesoporous structures due to the typical IV behaviors with H1 type hysteresis loops (Fig. S3). The specific surface areas are 82.87, 89.96, 76.45, and 71.39 m^2 g^{-1} for PCN, PCN-DP-0.1, PCN-DP-0.2, and PCN-DP-0.4, respectively. It can be found that the moderate doping of DP can improve the surface area of PCN. However, when further increasing amount of DP, the specific surface area of PCN-DP-x were decreased. This is mainly because excessive DP may destroy the inherent structure units of PCN and cause pore collapse, which could be examined by the reduction of pore volume from 0.48 to 0.35 cm^3 g^{-1} (Table 1).

The solid-state ^{13}C nuclear magnetic resonance (NMR) spectra of PCN, and PCN-DP-0.2 (Fig. 3a) exhibited two strong peaks at 156.6 and 164.5 ppm, which corresponded to the C-$(N)_3$ group and NH_2-$C(N)_2$ group in the heptazine units, respectively (Jiang et al., 2020). Interestingly, a peak at 163.0 ppm in the ^{13}C NMR spectra was found in PCN-DP-0.2 sample, which indicated carbon entities are hindered. This

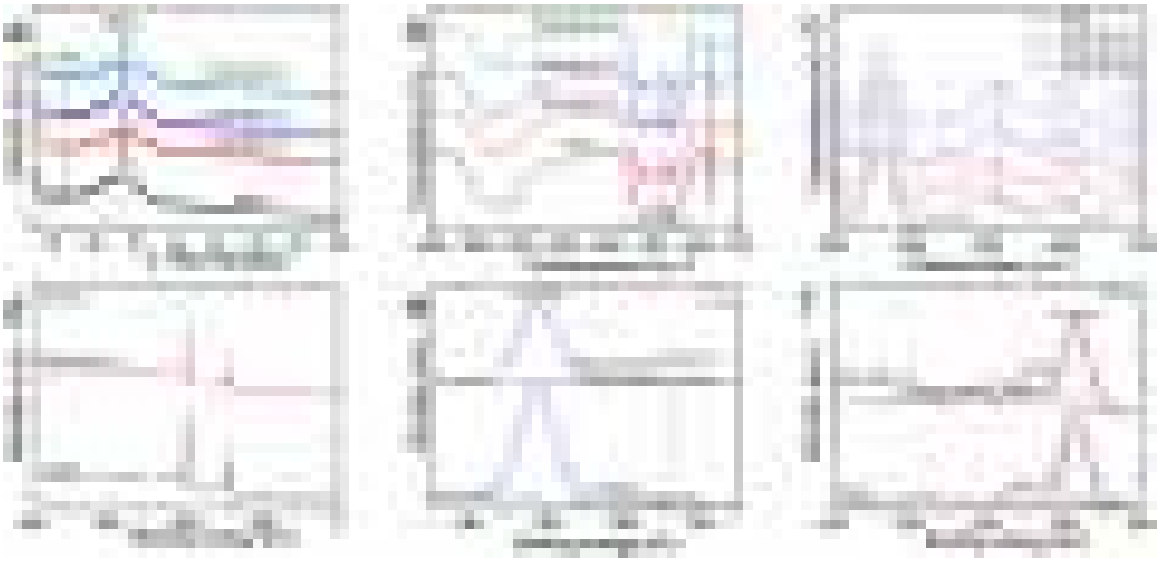

Fig. 1. (a) Powder XRD patterns, (b–c) FT-IR spectra of PCN and PCN-DP-x samples; high-resolution XPS spectra of (d) survey, (e) C 1s and (f) N 1s for PCN and PCN-DP-0.2.

distinct signal change indicates that the local chemical enviroments of carbon nitride are changed and the structural of PCN-DP-0.2 is not symmetric (Nimbalkar et al., 2019). Moreover, the electronic band structure of catalysts was studied by EPR spectra. As shown in Fig. 3b, PCN and PCN-DP-0.2 showed a paramagnetic absorption signals centered at a *g* value of 2.0036 in the magnetic field of 3260–3360 G, which was attributed to the presence of unpaired electrons in carbon nitride and an electron trapped on defects (Xu et al., 2019; Zhou et al., 2019c). The EPR signal of PCN-DP-0.2 was higher than PCN, indicating the concentration of unpaired electrons of PCN can be increased by pyrazine doping (Wang et al., 2020, 2019c). This result may also be due to defects caused by the doping of pyrazine.

It was expected that the incorporation of pyrazine into PCN might bring the modification of optical response. UV–vis diffuse reflection spectra of the PCN and PCN-DP-x samples are shown in Fig. 3c. The adsorption edge of PCN was around 460 nm, which originated from the π-π* electron transitions in the conjugated aromatic ring system. With the incorporation of DP, there are slight absorption tails in the range of

Table 1
Surface area and pore volume for PCN and PCN-DP samples.

Samples	Surface area (m^2 g^{-1})	Pore volume (cm^3 g^{-1})	Pore diameter (nm)
PCN	82.87	0.45	2.73
PCN-DP-0.1	89.96	0.48	2.74
PCN-DP-0.2	76.45	0.36	3.94
PCN-DP-0.4	71.39	0.34	2.74

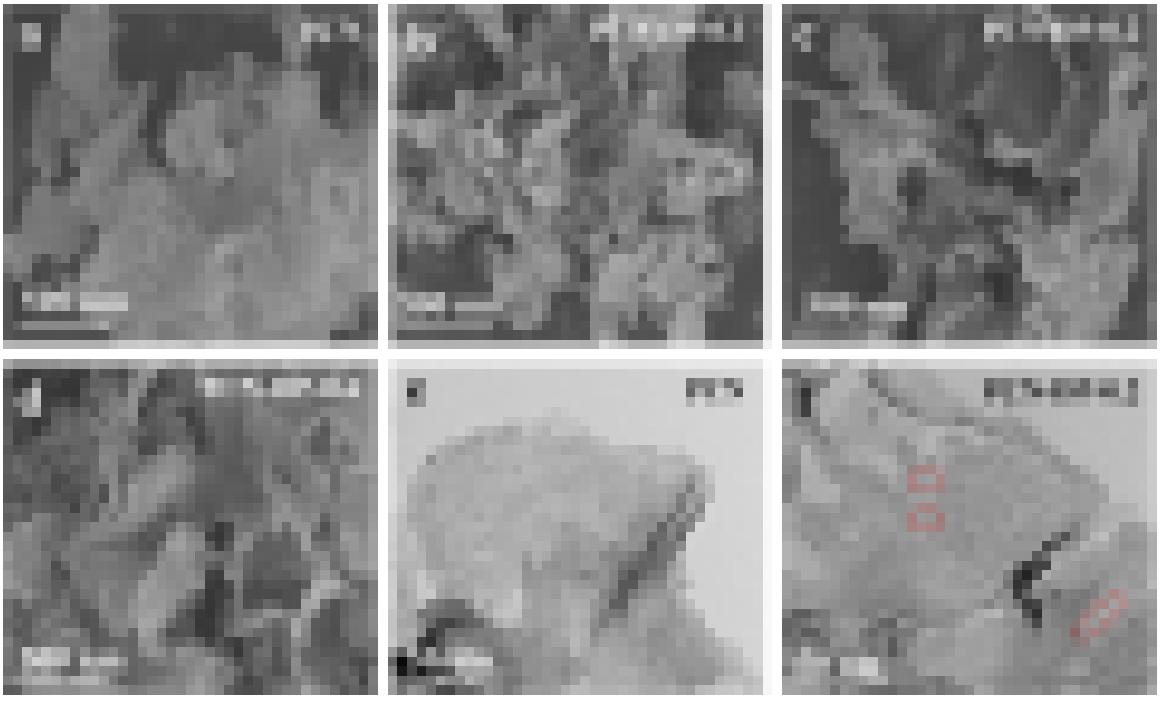

Fig. 2. SEM images of (a) PCN, (b) PCN-DP-0.1, (c) PCN-DP-0.2, and (d) PCN-DP-0.4. TEM images of (e) PCN and (f) PCN-DP-0.2.

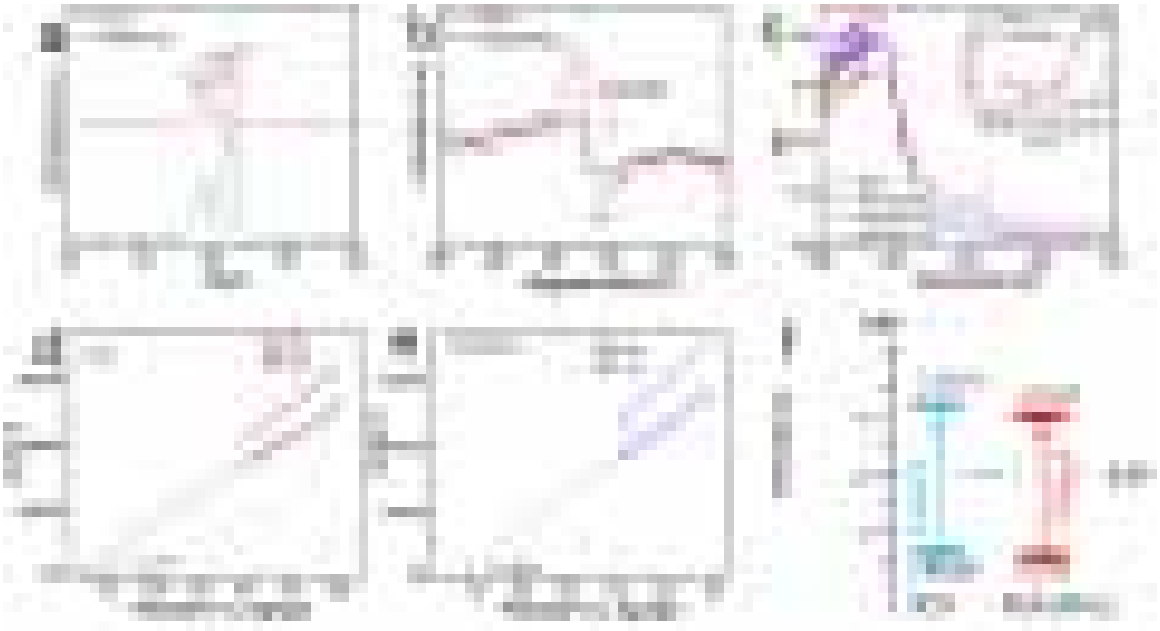

Fig. 3. (a) Solid-state ^{13}C MAS NMR spectra, (b) EPR spectra of PCN and PCN-DP-0.2, (c) UV–vis diffraction reflectance spectra of PCN and PCN-DP samples and the Tauc plots of PCN and PCN-DP-0.2 (inset), (d, e) Mott–Schottky plots, and (f) Schematic band structure of PCN and PCN-DP-0.2.

460～700 nm. The absorption tail gradually enhanced with the increased addition of DP. This new band may ascribed to the n-π* electron transition involving the lone pairs (Choi et al., 2018). Besides, the color change from yellow to brown suggested that the band gap was changed in PCN-DP samples. The band gap energy of PCN and PCN-DP-0.2 samples were measured to be 2.64 eV and 2.53 eV according to the Tauc plots (inset Fig. 3c), respectively. This reduced band gap of PCN-DP-0.2 indicated that this material effectively harvest wide range of visible light to produce more photogenerated charge carriers. This above change indicates that the introduction of pyrazine group can effectively improve visible light absorption and enhance the concentration of unpaired electrons, leading to the improved photocatalytic activity.

In addition, the conduction band position and valence band position are important for photocatalytic reaction. The flat band potential was measured by Mott–Schottky plots. As shown in Fig. 3d and e, the flat band potential (E_{fb}) of PCN and PCN-DP-0.2 were -1.41 V and -1.28 V vs. Ag/AgCl. Through the Nernst equation conversion, the E_{fb} of PCN and PCN-DP-0.2 were -0.86 eV and -0.73 eV vs. NHE (Yuan et al., 2018). Therefore, the conduction band of PCN and PCN-DP-0.2 were -1.16 eV and -1.03 eV. According to the band gap value, the valence band position of PCN and PCN-DP-0.2 were 1.48 eV and 1.5 eV. The band structure of PCN and PCN-DP-0.2 was given in Fig. 3f. It can be seen that the pyrazine coupling has effectively induced down-shift of VB position and CB position, respectively, thus decreasing the band gap energy. Although the CB position of PCN-DP-0.2 was decreased, but it still has enough reduction potential to induce the photocatalytic reaction.

3.2. Photocatalytic activity

To evaluate the validity of pyrazine doping strategy over PCN on improving photocatalytic activity, photocatalytic degradation of sulfamethazine (SMZ) were carried out over as-prepared samples. SMZ was chosen as the model pollutant since the SMZ is not photolyzed by visible light (Cheng et al., 2019b; Liu et al., 2019; Tian et al., 2019). Our previous studies indicated that the adsorption capacity of carbon nitride for SMZ was negligible (Zhou et al., 2018e, c). The control experiments and PCN samples were performed in Fig. 4a. When the mass of DP was 0.2 g, 99 % of SMZ could be degraded by the PCN-DP-0.2 under visible light irradiation in 60 min. By contrast, the pristine PCN only degraded 75 % of SMZ under the same condition. The corresponding pseudo-first order kinetic curve is exhibited in Fig. 4b. The apparent SMZ removal rate constants for PCN, PCN-DP-0.1, PCN-DP-0.2, and PCN-DP-0.4 were 0.023 min^{-1}, 0.051 min^{-1}, 0.087 min^{-1} and 0.065 min^{-1}, respectively. The degradation rate for PCN-DP-0.2 was about 4 times than that of the PCN. After normalized with their BET specific surface areas, the activity of PCN-DP-0.2 (1.14 mg min^{-1} m^{-2}) was still higher than those of PCN (0.27 mg min^{-1} m^{-2}), PCN-DP-0.1 (0.57 mg min^{-1} m^{-2}), and PCN-DP-0.4 (0.91 mg min^{-1} m^{-2}) (Wang et al., 2017). Moreover, compared with some existing photocatalysts (i.e. Bi_2WO_6, $Bi_2O_{17}Cl_2$, g-C_3N_4), the PCN-DP-x generally showed excellent photocatalytic activity (Table S2).

Liquid chromatography-mass spectrometer (LC—MS) was used to identify the degradation products of SMZ and two major intermediates were found. The LC spectra indicated that the peak intensity of SMZ (t = 9.427 min) was decreased with the reaction time prolonging (Fig. 4c). The peak at 1.229 min and 2.283 min may be attributed to the degradation intermediates of SMZ. Detailed MS graph was provided in Fig. S4. As shown in Fig. 4d, the product ion at *m/z* 279 was the SMZ. The one intermediate P1 was *m/z* 215, corresponding to 4-(2-imino-4,6-dimethylpyrimidin-1(2 H)-yl) aniline. This product was generated by smiles-type rearrangement followed by SO_2 extrusion (Fan et al., 2015b). Recent studies have been reported the formation of this product. The concentration of *m/z* 215 was formed in the first 15 min. When the reaction progressed, the concentration of P1 was remained stable in 15－45 min, and then decreased in 60 min. The other important intermediate P2 was *m/z* 124, corresponding to 2-amino-4,6-dimethylpyrimidine. The formation of P2 was formed by sulfonamide bond cleavage since the sulfonamide antibiotics can oxidized by reactive oxygen species. The concentration of P2 was produced rapidly, but they keep constant in a low level with the time prolonging. The proposed SMZ degradation products were presented in Table S3.

Previous studies indicated that the solution pH could influence the generation of oxidative species in the photodegradation process. Fig. S5 indicated that the degradation rates of SMZ were increased with the augmentation of initial pH. At low pH conditions, $^{\cdot}O_2^-$ may prefer to combine with H^+ to form H_2O_2, which inhibits the degradation of SMZ

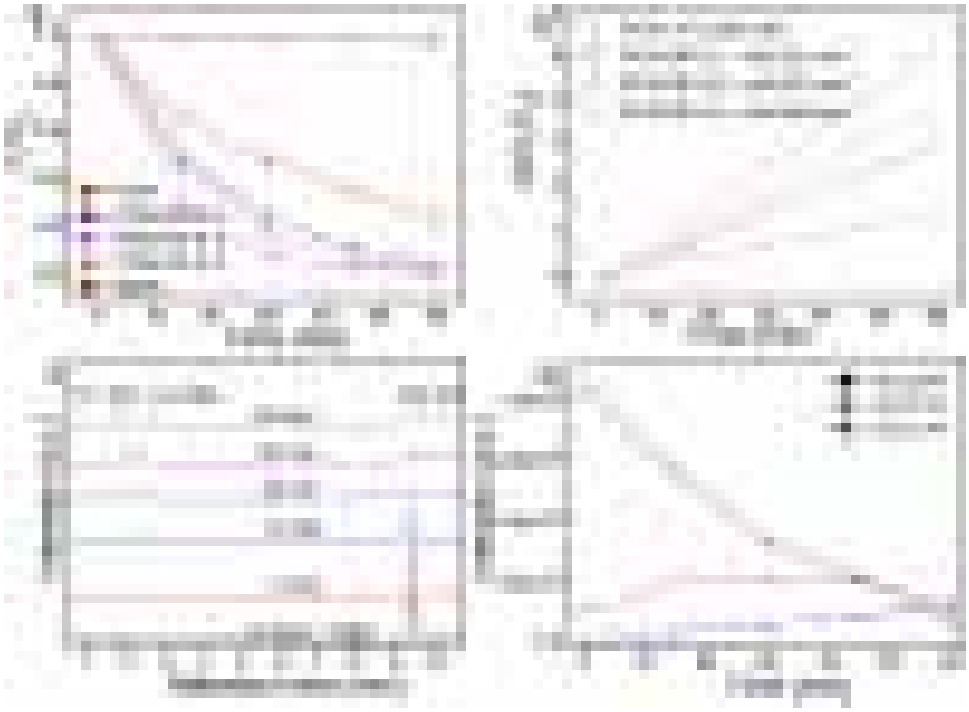

Fig. 4. (a) Photocatalytic degradation of SMZ, (b) degradation rate of SMZ on PCN and PCN-DP-x samples, (c) LC spectrum of SMZ solution degraded by PCN-DP-0.2, and (d) Evolution of the product ions and decrease of SMZ in the photocatalytic degradation of SMZ over PCN-DP-0.2.

(Song et al., 2017). Fig. S6a showed that the SMZ degradation rate by PCN-DP-0.2 was slightly dropped from 0.087 min^{-1} to 0.078 min^{-1} after four cycles. This decrease of degradation efficiency may attribute to the degradation products covering the active sites of catalyst. In addition, after cycle photocatalytic reactions, the used PCN-DP-0.2 sample was further characterized by XRD, TEM and XPS. As shown in Fig. S6b-f, no noticeable changes in the crystal, morphology, and surface structure are found, which suggests the high stability of pyrazine modified photocatalyst in the SMZ degradation system.

This modification strategy was also enhances the photocatalytic H_2 evolution activity since more photoelectrons are available over pyrazine doping PCN (Jin et al., 2018). As shown in Fig. 5a, all samples are active for H_2 evolution with visible light illumination. The optimized sample (PCN-DP-0.2) exhibited best photocatalytic efficiency among all photocatalysts studied. The average H_2 evolution rate of PCN-DP-0.2 reaching up to 63 μmol h^{-1}, is almost 6.3 times in comparison with that of pristine PCN (10 μmol h^{-1}). When excessive pyrazine was doped, an adverse effect about H_2 evolution was emerged due to the excessive foreign units may destruct the conjugated framework. The stability of PCN-DP-0.2 was evaluated for a long-term photocatalytic reaction (Fig. 5b), in which slight decrease of photocatalytic activity was observed after four cycles, indicating PCN-DP-0.2 possessed excellent stability. The TEM image of PCN-Pt and PCN-DP-0.2-Pt was presented in Fig. 5c and d–e, respectively, which indicated that the Pt particles of small size are much more evenly dispersed on the surface of PCN-DP-0.2 sample. Furthermore, the results of XPS and TEM image for the fresh and used PCN-DP-0.2 indicated that the as-prepared sample are chemically stable (Fig. S7). These above results indicated that our strategy was simple and the as-prepared photocatalysts have higher photocatalytic activity (Wang et al., 2018; Zhang et al., 2017).

3.3. Mechanism of the enhanced photocatalytic activity

Carbon materials have excellent electrical conductivity. So, we think that pyrazine in the structure of PCN can act an electron channel and quicker transfer the electrons than the original layer. The efficient separation of electron-hole pairs was further demonstrated by photocurrent measurements and electrochemical impedance spectroscopy (EIS) (Yi et al., 2019). Fig. 6a showed that both samples exhibited stable photocurrents during the light on and off cycles. Among these samples, the photocurrent of PCN-DP-0.2 was 3 times higher than that of the PCN, suggesting that more efficient separation of photogenerated charge carriers was achieved. Meanwhile, compared with PCN, all the modified samples showed a smaller semicircular Nyquist plots diameter (Fig. 6b), suggesting a charge transfer resistance, and leading to more efficient separation of photogenerated charge carriers. It can be seen that the DP doping is beneficial for the separation and transfer of photogenerated carriers.

The separation rates of charge carriers in carbon nitride were investigated by photo-luminescence (PL) test. As shown in Fig. 7a, the peak at 460 nm of PCN was assigned to the band-to-band layer recombination of photogenerated carriers. Remarkable PL quenching of this peak was obtained in PCN-DP samples (from 460 nm to 470 nm), indicating the recombination of charge carriers was restricted in PCN-DP samples. Moreover, the pyrazine can be acted as a hyperchannel to transfer the photogenerated electrons, which was beneficial for electron-holes separation. Time-resolved fluorescence decay spectroscopy (TRPL) was further to demonstrate it. Fig. 7b and Table S4 suggested the lifetime of PCN-DP-0.2 (5.64 ns) was shorter than that of the PCN (8.34 ns). This decreased lifetime indicated that the exciton dissociation was improved by pyrazine doping (Qin et al., 2019). PL quenching was further examined by the photographs of PCN and PCN-DP-0.2 powders or their suspensions in water with UV light illumination. As shown in Fig. 7c, compared with the PCN, the PCN-DP-0.2 displayed much lower intensity of luminescence obviously in powder and suspensions, which was in consistent with the results of PL (Li and Zhang, 2018).

ESR measurements and trapping experiments were carried out to demonstrate photodegradation mechanism of SMZ by PCN and PCN-DP-0.2. As shown in Fig. 8a, no signal of DMPO-$^{\cdot}O_2^-$ was detected in dark for both PCN and PCN-DP-0.2 samples. The signal of DMPO-$^{\cdot}O_2^-$ (an intensity ratio of 1:1:1:1 signal) was increased with the increase of irradiation time. Moreover, the intensity signals of DMPO-$^{\cdot}O_2^-$ for PCN-DP-0.2 was higher than PCN those of the PCN in 4 min and 8 min visible light irradiation, respectively. Meanwhile, the signal of DMPO-

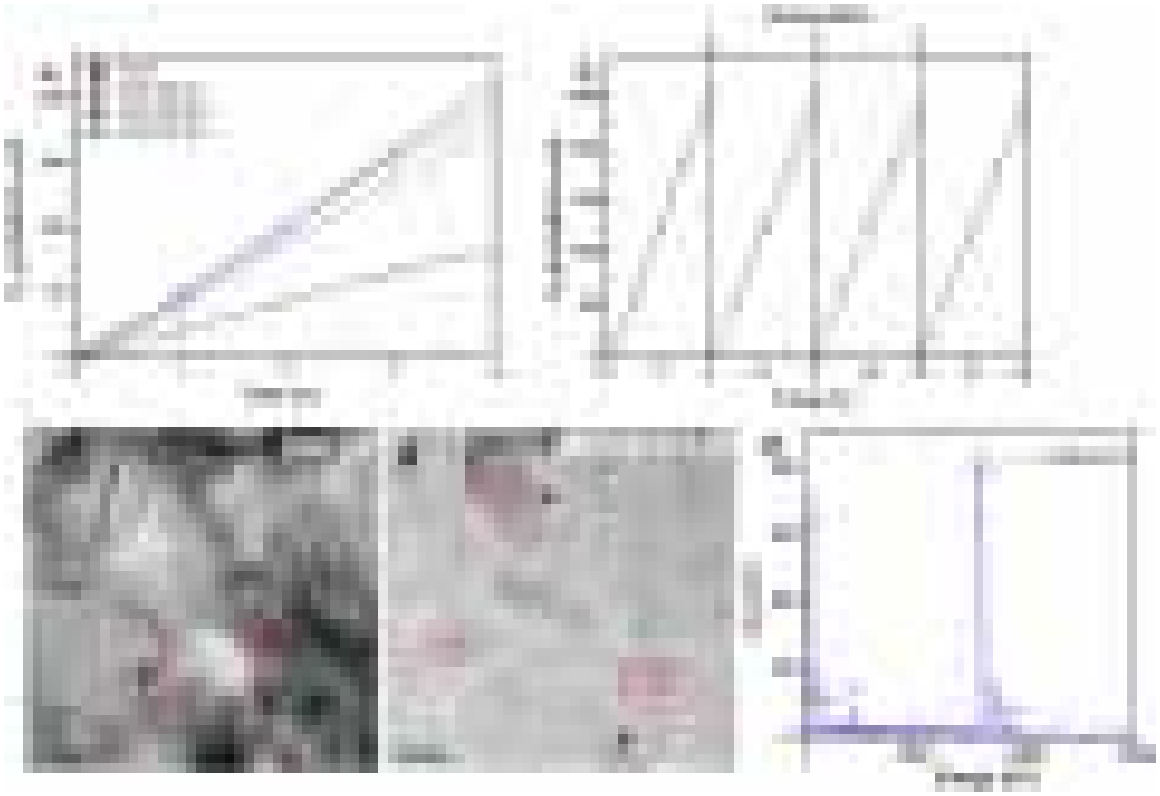

Fig. 5. (a) Photocatalytic H_2 evolution performance for PCN and PCN-DP-x samples, (b) cycle measurements of H_2 evolution of PCN-DP-0.2, (c) TEM image of Pt deposited PCN, (d) TEM image of Pt deposited PCN-DP-0.2 and (e) EDS of Pt deposited PCN-DP-0.2.

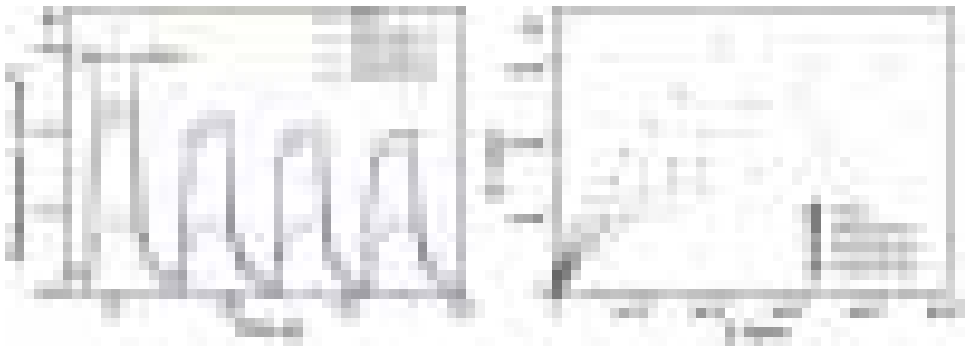

Fig. 6. (a) Photocurrent response curves and (b) EIS Nyquist plot of PCN and PCN-DP-x samples.

•OH (an intensity ratio of 1:2:2:1 signal) was obviously detected in the DMPO water solution for PCN-DP-0.2 (Fig. 8b). However, the signal of DMPO-•OH for PCN was too weak to be detected. Furthermore, trapping experiments by different scavengers (IPA for •OH, CAT for H_2O_2, TEMPOL for $^{\cdot}O_2^-$, and EDTA for h^+) were carried out. As shown in Fig. 8c and d, the addition of TEMPOL and EDTA inhibited 84.6 % and 62.4 % of SMZ degradation, respectively, indicating that the $^{\cdot}O_2^-$ and h^+ mainly accounted for the SMZ degradation. About 30 % of SMZ degradation was suppressed in the presence of CAT, suggesting that H_2O_2 had a positive effect for photocatalytic degradation of SMZ. IPA showed no significant impact on the SMZ photodegradation. This result indicated that the main active species were $^{\cdot}O_2^-$ and h^+. Therefore, the main effect of pyrazine doping in PCN seems to accelerated the conduction band (CB) electron transfer to O_2 with generating more $^{\cdot}O_2^-$ and O˙H for reaction.

Combining the above results, the possible pathways of PCN-DP for SMZ degradation (system I) and H_2 evolution (system II) were proposed in Scheme 1. Evidently, the electronic structure is largely modified by the incorporation of pyrazine molecules due to the doping can alter the thermal polymerization route. Pyrazine can act as electron-acceptor to separation the charge carrier combination of PCN-DP. Under visible light irradiation, the catalyst was excited, and then generated electrons and holes. In the system I, the photocatalytic degradation of SMZ by PCN-DP was attributed to reactive oxygen species (such as $^{\cdot}O_2^-$, H_2O_2 and O˙H) and the interfacial interactions of contaminant with photocatalysts. The distorted structure and widen visible light absorption enhanced the migration efficiency of photogenerated electrons, causing a high yield of $^{\cdot}O_2^-$. In addition, the holes can directly decompose the pollutants. For the water splitting (system II), since the band structure of PCN-DP was modified, which make more photogenerated carriers generated from it. Pt particles are evenly dispersed on the surface of PCN-DP-0.2 sample due to the pyrazine channel. The synergistic effect of Pt and pyrazine channel induces the high activity of H_2 evolution for PCN-DP-0.2 sample.

3.4. Phytotoxicity measurements results

Seed germination and radicle elongation tests are usually used to

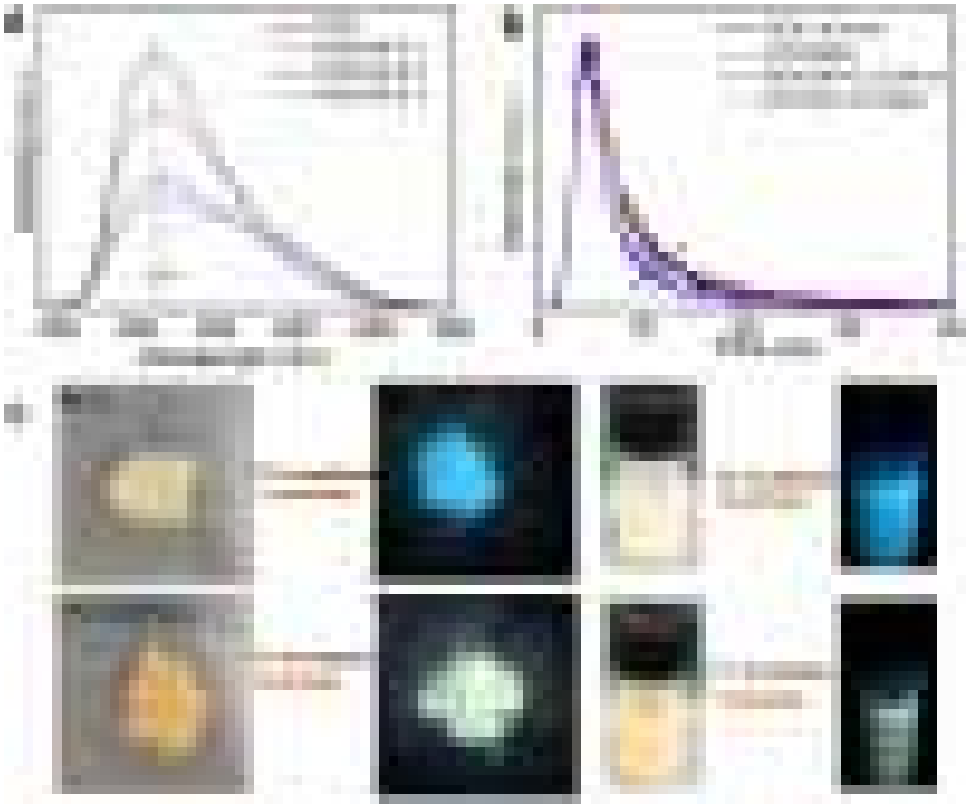

Fig. 7. (a) Room temperature steady state photoluminescence (PL) emission spectra, (b) time-resolved fluorescence decay spectra of PCN and PCN-DP-x sample with an excitation wavelength of 365 nm, (c) Photographs of PCN and PCN-DP-0.2 powders and suspensions under 365 nm irradiation.

assess the plant toxicity of contaminants and contaminated environment (Moreira et al., 2019). In this study, Chinese cabbage (Brassica rapa L.) was choose since its seed has the advantages of uniform size (1 − 2 mm), rapid germination and is sensitive to antibiotics. In the seed germination stage, Chinese cabbage seeds began to germinate after 8 h. As shown in Fig. 9a and Fig. S8, the germination percentage of control and treatments generally reached over 92 % after 24 h of incubation, respectively. The results of the phytotoxicity experiments exhibited that sulfamethazine (SMZ) solution or photocatalyst had no universal effect on seed germination stage. This may be ascribed to seed coat on the

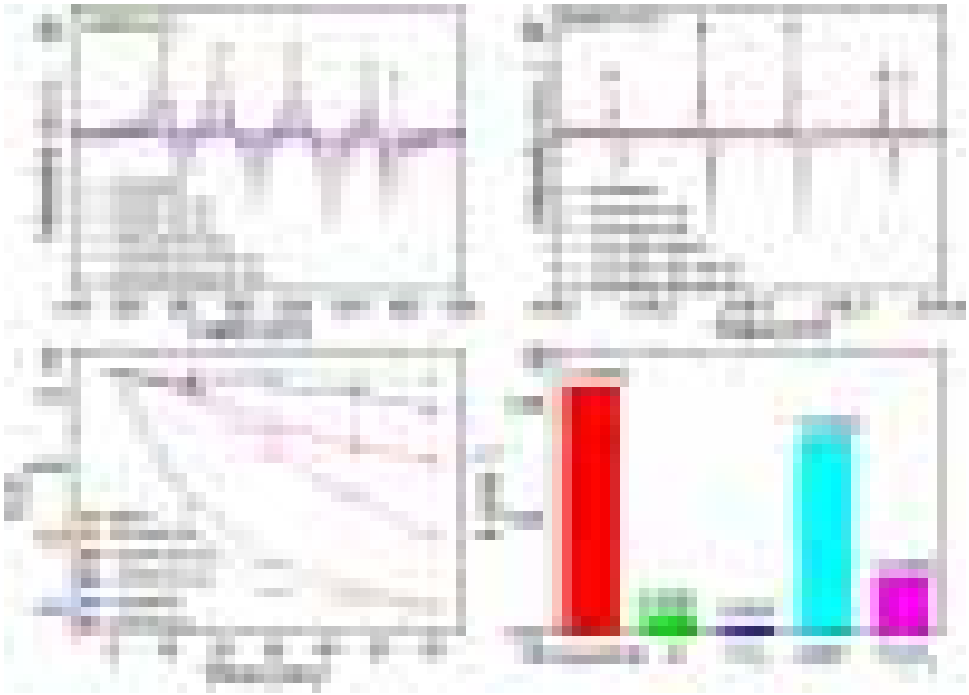

Fig. 8. ESR signals of (a) DMPO-$^{\cdot}O_2^-$ adducts in methanol dispersion and (b) DMPO-$^{\cdot}$OH adducts in methanol dispersion over PCN and PCN-DP-0.2, (c and d) reactive species trapping experiments of PCN-DP-0.2 under visible light irradiation.

Scheme 1. Possible pathway of PCN-DP for SMZ degradation (system I) and H_2 evolution (system II).

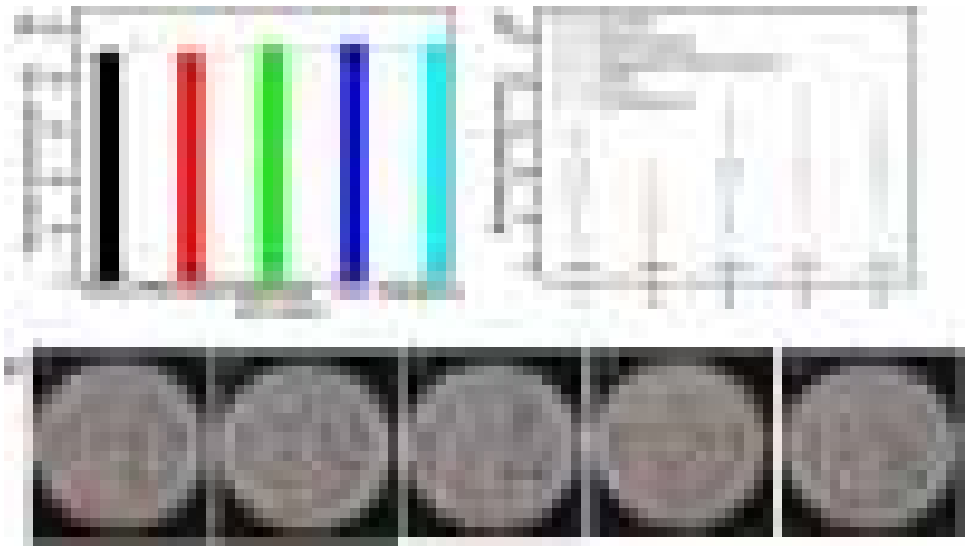

Fig. 9. (a) Effect of SMZ solution and photocatalyst on seed germination for 24 h (n = 160), (b) Effect of SMZ solution and photocatalyst on Chinese cabbage seeds radicle length for another 24 h (n = 80). Boxes illustrate the first quartile, median and third quartile of the data. The mean is marked with a dotted line in the box. The ends of the whiskers represent the 5th percentile and the 95th percentile. Values beyond 1.5 times the box height are outliers plotted as circles. (c) Micrograph of seed radicle elongation stage.

embryo of seeds. In the radicle elongation stage, the seed radicle length in SMZ solution (mean length of 8.89 mm, n = 80) was obviously lower than that the blank sample (mean length of 14.76 mm, n = 80) (Fig. 9b and c). However, the degraded SMZ solution (after photocatalysis by PCN-DP) showed no inhibition on seed radicle length (mean length of 16.11 mm, n = 80). In addition, the PCN and PCN-DP-0.2 samples showed no influence on radicle elongation. This result indicated that the toxicity of SMZ polluted water after degradation is greatly reduced, and the treated water is clean and environmentally friendly. Moreover, the as-prepared photocatalysts are environmentally friendly.

4. Conclusions

In summary, a highly efficient photocatalyst was prepared via a bottom-up method, which involves pyrazine doping, thermal-induced exfoliation and condensation/polymerization. Both morphology and electronic structures of pyrazine doped PCN were greatly modified via molecule doping of pyrazine. The electron-deficiency pyrazine can acted as a hyperchannel to transfer the photogenerated electrons, which was beneficial for electron-holes separation. As a result, an overall enhanced SMZ degradation rate and H_2 production rate of PCN-DP were achieved, which was consistent with the extended visible light absorption. The photocatalytic degradation of SMZ by PCN-DP was attributed to reactive oxygen species (such as $^{\cdot}O_2^-$, H_2O_2 and $^{\cdot}OH$) and the interfacial interactions of pollutant with photocatalysts. In addition, Phytotoxicity experiments were conducted, which shows that the toxicity of sulfamethazine after degradation is greatly reduced and the as-prepared photocatalyst is environmentally friendly. Although some achievements have been made, the problem of catalyst recovery is still involved, further optimization is needed.

Statement of contributions

C.Y. Zhou, D.L. Huang and I designed the project; C.Y. Zhou, Y. Luo, Y. Yang, M. Cheng, and Y. Liu carried out the assays and wrote the paper; the data were mainly processed by C. Lai and B. Song; W.P. Xiong, B.B. Shao, Z. H. Li and I polished this paper.

Declaration of Competing Interest

The authors declare that they have no known competing financial interests or personal relationships that could have appeared to influence the work reported in this paper.

Acknowledgements

This study was financially supported by the Program for the National Natural Science Foundation of China (81773333, 51879101, 51809090, 51579098, 51779090, 51709101, 51709100, 51278176, 51521006, 51378190), the National Program for Support of Top-Notch Young Professionals of China (2014), the Fundamental Research Funds for the Central Universities, Hunan Provincial Science and Technology

Plan Project (No. 2016RS3026, 2017SK2243, 2018SK20410), the Program for New Century Excellent Talents in University (NCET-13-0186), the Fundamental Research Funds for the Central Universities (531109200027, 531107051080, 531107050978, 531107051205), Shanghai Tongji Gao Tingyao Environmental Science and Technology Development Foundation, and the Program for Changjiang Scholars and Innovative Research Team in University (IRT-13R17).

Appendix A. Supplementary data

Supplementary material related to this article can be found, in the online version, at doi:https://doi.org/10.1016/j.jhazmat.2019.121947.

References

Bolong, N., Ismail, A., Salim, M.R., Matsuura, T., 2009. A review of the effects of emerging contaminants in wastewater and options for their removal. Desalination 239, 229–246.
Chen, N., Huang, Y., Hou, X., Ai, Z., Zhang, L., 2017. Photochemistry of hydrochar: reactive oxygen species generation and sulfadimidine degradation. Environ. Sci. Technol. 51, 11278–11287.
Cheng, J., Hu, Z., Lv, K., Wu, X., Li, Q., Li, Y., Li, X., Sun, J., 2018. Drastic promoting the visible photoreactivity of layered carbon nitride by polymerization of dicyandiamide at high pressure. Appl. Catal. B: Environ. 232, 330–339.
Cheng, J., Hu, Z., Li, Q., Li, X., Fang, S., Wu, X., Li, M., Ding, Y., Liu, B., Yang, C., 2019a. Fabrication of high photoreactive carbon nitride nanosheets by polymerization of amidinourea for hydrogen production. Appl. Catal. B: Environ. 245, 197–206.
Cheng, M., Liu, Y., Huang, D., Lai, C., Zeng, G., Huang, J., Liu, Z., Zhang, C., Zhou, C., Qin, L., 2019b. Prussian blue analogue derived magnetic Cu-Fe oxide as a recyclable photo-Fenton catalyst for the efficient removal of sulfamethazine at near neutral pH values. Chem. Eng. J. 362, 865–876.
Choi, C.H., Lin, L., Gim, S., Lee, S., Kim, H., Wang, X., Choi, W., 2018. Polymeric Carbon Nitride with Localized Aluminum Coordination Sites as a Durable and Efficient Photocatalyst for Visible Light Utilization. ACS Catal. 8, 4241–4256.
Dong, G., Fan, H., Fu, K., Ma, L., Zhang, S., Zhang, M., Ma, J., Wang, W., 2019. The evaluation of super-capacitive performance of novel g-C_3N_4/PPy nanocomposite electrode material with sandwich-like structure. Compos Part B: Eng. 162, 369–377.
Duan, Y., Li, X., Lv, K., Zhao, L., Liu, Y., 2019. Flower-like g-C_3N_4 assembly from holy nanosheets with nitrogen vacancies for efficient NO abatement. Appl. Surf. Sci. 492, 166–176.
Fan, X., Zhang, L., Cheng, R., Wang, M., Li, M., Zhou, Y., Shi, J., 2015a. Construction of graphitic C_3N_4-based intramolecular donor–acceptor conjugated copolymers for photocatalytic hydrogen evolution. ACS Catal. 5, 5008–5015.
Fan, Y., Ji, Y., Kong, D., Lu, J., Zhou, Q., 2015b. Kinetic and mechanistic investigations of the degradation of sulfamethazine in heat-activated persulfate oxidation process. J. Hazard. Mater. 300, 39–47.
Gong, J.-L., Wang, B., Zeng, G.-M., Yang, C.-P., Niu, C.-G., Niu, Q.-Y., Zhou, W.-J., Liang, Y., 2009. Removal of cationic dyes from aqueous solution using magnetic multi-wall carbon nanotube nanocomposite as adsorbent. J. Hazard. Mater. 164, 1517–1522.
He, K., Chen, G., Zeng, G., Chen, A., Huang, Z., Shi, J., Huang, T., Peng, M., Hu, L., 2018. Three-dimensional graphene supported catalysts for organic dyes degradation. Appl. Catal. B: Environ. 228, 19–28.
Huang, D., Yan, X., Yan, M., Zeng, G., Zhou, C., Wan, J., Cheng, M., Xue, W., 2018. Graphitic carbon nitride-based heterojunction photoactive nanocomposites: applications and mechanism insight. ACS Appl. Mater. Interfaces 10, 21035–21055.
Huang, D., Chen, S., Zeng, G., Gong, X., Zhou, C., Cheng, M., Xue, W., Yan, X., Li, J., 2019a. Artificial Z-scheme photocatalytic system: What have been done and where to go? Coord. Chem. Rev. 385, 44–80.
Huang, D., Li, J., Zeng, G., Xue, W., Chen, S., Li, Z., Deng, R., Yang, Y., Cheng, M., 2019b. Facile construction of hierarchical flower-like Z-scheme AgBr/Bi_2WO_6 photocatalysts for effective removal of tetracycline: Degradation pathways and mechanism. Chem. Eng. J., 121991.
Huang, D., Li, Z., Zeng, G., Zhou, C., Xue, W., Gong, X., Yan, X., Chen, S., Wang, W., Cheng, M., 2019c. Megamerger in photocatalytic field: 2D g-C_3N_4 nanosheets serve as support of 0D nanomaterials for improving photocatalytic performance. Appl. Catal. B: Environ. 240, 153–173.
Jiang, D., Chen, M., Wang, H., Zeng, G., Huang, D., Cheng, M., Liu, Y., Xue, W., Wang, Z., 2019. The application of different typological and structural MOFs-based materials for the dyes adsorption. Coord. Chem. Rev. 380, 471–483.
Jiang, L., Li, J., Wang, K., Zhang, G., Li, Y., Wu, X., 2020. Low boiling point solvent mediated strategy to synthesize functionalized monolayer carbon nitride for superior photocatalytic hydrogen evolution. Appl. Catal. B: Environ. 260, 118181.
Jin, X., Zhang, L., Fan, X., Tian, J., Wang, M., Shi, J., 2018. A photo-excited electron transfer hyperchannel constructed in Pt-dispersed pyrimidine-modified carbon nitride for remarkably enhanced water-splitting photocatalytic activity. Appl. Catal. B: Environ. 237, 888–894.
Kim, H., Gim, S., Jeon, T.H., Kim, H., Choi, W., 2017. Distorted carbon nitride structure with substituted benzene moieties for enhanced visible light photocatalytic activities. ACS Appl. Mater. Interfaces 9, 40360–40368.
Li, Z., Zhou, S., Yang, Q., Zhang, Z., Fang, X., 2019. Insight into the Enhanced Hydrogen Evolution Activity of 2, 4-Diaminopyrimidine-Doped Graphitic Carbon Nitride Photocatalysts. J. Phys. Chem. C 123, 2228–2237.
Li, Y., Gu, M., Shi, T., Cui, W., Zhang, X., Dong, F., Cheng, J., Fan, J., Lv, K., 2020. Carbon vacancy in C_3N_4nanotube: Electronic structure, photocatalysis mechanism and highly enhanced activity. Appl. Catal. B: Environ. 262, 118281.
Li, K., Zhang, W.-D., 2018. Creating graphitic carbon nitride based Donor-π–Acceptor-π–Donor structured catalysts for highly photocatalytic hydrogen evolution. Small 14, 1703599.
Linsebigler, A.L., Lu, G., Yates Jr, J.T., 1995. Photocatalysis on TiO_2 surfaces: principles, mechanisms, and selected results. Chem. Rev. 95, 735–758.
Liu, Y., Zeng, G., Zhong, H., Wang, Z., Liu, Z., Cheng, M., Liu, G., Yang, X., Liu, S., 2017. Effect of rhamnolipid solubilization on hexadecane bioavailability: enhancement or reduction? J. Hazard. Mater. 322, 394–401.
Liu, Y., Liu, Z., Huang, D., Cheng, M., Zeng, G., Lai, C., Zhang, C., Zhou, C., Wang, W., Jiang, D., 2019. Metal or metal-containing nanoparticle@ MOF nanocomposites as a promising type of photocatalyst. Coord. Chem. Rev. 388, 63–78.
Luo, Y., Liang, J., Zeng, G., Li, X., Chen, M., Jiang, L., Xing, W., Tang, N., Fang, Y., Chen, X., 2019. Evaluation of tetracycline phytotoxicity by seed germination stage and radicle elongation stage tests: A comparison of two typical methods for analysis. Environ. pollut. 251, 257–263.
Ming, J., Liu, A., Zhao, J., Zhang, P., Huang, H., Lin, H., Xu, Z., Zhang, X., Wang, X., Hofkens, J., Roeffaers, M.B.J., Long, J., 2019. Hot π-Electron tunneling of metal–Insulator–COF nanostructures for efficient hydrogen production. Angew. Chem. Int. Ed. 58, 18290–18294.
Moreira, N.F.F., Sampaio, M.J., Ribeiro, A.R., Silva, C.G., Faria, J.L., Silva, A.M.T., 2019. Metal-free g-C_3N_4 photocatalysis of organic micropollutants in urban wastewater under visible light. Appl. Catal. B: Environ. 248, 184–192.
Nimbalkar, D.B., Stas, M., Hou, S.-S., Ke, S.-C., Wu, J.-J., 2019. Microscopic revelation of charge-trapping sites in polymeric carbon nitrides for enhanced photocatalytic activity by correlating with chemical and electronic structures. ACS Appl. Mater. Interfaces 11, 19087–19095.
Ong, W.J., Tan, L.L., Ng, Y.H., Yong, S.T., Chai, S.P., 2016. Graphitic Carbon Nitride (g-C_3N_4)-Based Photocatalysts for Artificial Photosynthesis and Environmental Remediation: Are We a Step Closer To Achieving Sustainability? Chem. Rev. 116, 7159–7329.
Qin, L., Yi, H., Zeng, G., Lai, C., Huang, D., Xu, P., Fu, Y., He, J., Li, B., Zhang, C., 2019. Hierarchical porous carbon material restricted Au catalyst for highly catalytic reduction of nitroaromatics. J. Hazard. Mater. 380, 120864.
Shimizu, A., Takada, H., Koike, T., Takeshita, A., Saha, M., Nakada, N., Murata, A., Suzuki, T., Suzuki, S., Chiem, N.H., 2013. Ubiquitous occurrence of sulfonamides in tropical Asian waters. Sci. Total Environ. 452, 108–115.
Song, Y., Tian, J., Gao, S., Shao, P., Qi, J., Cui, F., 2017. Photodegradation of sulfonamides by g-C_3N_4 under visible light irradiation: effectiveness, mechanism and pathways. Appl. Catal. B: Environ. 210, 88–96.
Song, B., Chen, M., Ye, S., Xu, P., Zeng, G., Gong, J., Li, J., Zhang, P., Cao, W., 2019. Effects of multi-walled carbon nanotubes on metabolic function of the microbial community in riverine sediment contaminated with phenanthrene. Carbon 144, 1–7.
Sprick, R.S., Jiang, J.X., Bonillo, B., Ren, S., Ratvijitvech, T., Guiglion, P., Zwijnenburg, M.A., Adams, D.J., Cooper, A.I., 2015. Tunable organic photocatalysts for visible-light-driven hydrogen evolution. J. Am. Chem. Soc. 137, 3265–3270.
Tian, S., Zhang, C., Huang, D., Wang, R., Zeng, G., Yan, M., Xiong, W., Zhou, C., Cheng, M., Xue, W., 2019. Recent progress in sustainable technologies for adsorptive and reactive removal of sulfonamides. Chem. Eng. J., 123423.
Tong, Z., Yang, D., Li, Z., Nan, Y., Ding, F., Shen, Y., Jiang, Z., 2017. Thylakoid-Inspired Multishell g-C_3N_4 Nanocapsules with Enhanced Visible-Light Harvesting and Electron Transfer Properties for High-Efficiency Photocatalysis. ACS Nano 11, 1103–1112.
Utterback, J.K., Grennell, A.N., Wilker, M.B., Pearce, O.M., Eaves, J.D., Dukovic, G., 2016. Observation of trapped-hole diffusion on the surfaces of CdS nanorods. Nat. Chem. 8, 1061.
Wang, C.-Y., Zhang, X., Qiu, H.-B., Huang, G.-X., Yu, H.-Q., 2017. $Bi_{24}O_{31}Br_{10}$ nanosheets with controllable thickness for visible–light–driven catalytic degradation of tetracycline hydrochloride. Appl. Catal. B: Environ. 205, 615–623.
Wang, H., Wu, Y., Feng, M., Tu, W., Xiao, T., Xiong, T., Ang, H., Yuan, X., Chew, J.W., 2018. Visible-light-driven removal of tetracycline antibiotics and reclamation of hydrogen energy from natural water matrices and wastewater by polymeric carbon nitride foam. Water Res. 144, 215–225.
Wang, H., Zeng, Z., Xu, P., Li, L., Zeng, G., Xiao, R., Tang, Z., Huang, D., Tang, L., Lai, C., 2019a. Recent progress in covalent organic framework thin films: fabrications, applications and perspectives. Chem. Soc. Rev. 48, 488–516.
Wang, W., Zeng, Z., Zeng, G., Zhang, C., Xiao, R., Zhou, C., Xiong, W., Yang, Y., Lei, L., Liu, Y., Huang, D., Cheng, M., Yang, Y., Fu, Y., Luo, H., Zhou, Y., 2019b. Sulfur doped carbon quantum dots loaded hollow tubular g-C_3N_4 as novel photocatalyst for destruction of Escherichia coli and tetracycline degradation under visible light. Chem. Eng. J. 378, 122132.
Wang, K., Li, J., Zhang, G., 2019c. Ag-Bridged Z-Scheme 2D/2D Bi5FeTi3O15/g-C_3N_4 heterojunction for enhanced photocatalysis: mediator-induced interfacial charge transfer and mechanism insights. ACS Appl. Mater. Interfaces 11, 27686–27696.
Wang, K., Li, Y., Li, J., Zhang, G., 2020. Boosting interfacial charge separation of $Ba_5Nb_4O_{15}$/g-C_3N_4 photocatalysts by 2D/2D nanojunction towards efficient visible-light driven H2 generation. Appl. Catal. B: Environ. 263, 117730.
Wen, Y., Fan, H., Ning, L., Wang, C., Hu, B., Ma, J., Wang, W., Cui, K., 2019. Graphitic carbon nitride nanosheets prepared by gaseous molecules assembling for enhanced photocatalytic performance. J. Mater. Sci. 54, 1462–1474.
Wu, X., Cheng, J., Li, X., Li, Y., Lv, K., 2019. Enhanced visible photocatalytic oxidation of NO by repeated calcination of g-C_3N_4. Appl. Surf. Sci. 465, 1037–1046.
Xia, Q., Wang, H., Huang, B., Yuan, X., Zhang, J., Zhang, J., Jiang, L., Xiong, T., Zeng, G., 2019. State-of-the-Art Advances and Challenges of Iron-Based Metal Organic

Frameworks from Attractive Features, Synthesis to Multifunctional Applications. Small 15, 1803088.
Xing, W., Chen, G., Li, C., Han, Z., Hu, Y., Meng, Q., 2018. Doping effect of non-metal group in porous ultrathin g-C_3N_4 nanosheets towards synergistically improved photocatalytic hydrogen evolution. Nanoscale 10, 5239–5245.
Xiong, W., Zeng, Z., Li, X., Zeng, G., Xiao, R., Yang, Z., Zhou, Y., Zhang, C., Cheng, M., Hu, L., 2018. Multi-walled carbon nanotube/amino-functionalized MIL-53 (Fe) composites: remarkable adsorptive removal of antibiotics from aqueous solutions. Chemosphere 210, 1061–1069.
Xu, P., Zeng, G.M., Huang, D.L., Feng, C.L., Hu, S., Zhao, M.H., Lai, C., Wei, Z., Huang, C., Xie, G.X., Liu, Z.F., 2012. Use of iron oxide nanomaterials in wastewater treatment: a review. Sci. Total Environ. 424, 1–10.
Xu, J., Luo, L., Xiao, G., Zhang, Z., Lin, H., Wang, X., Long, J., 2014. Layered $C_3N_3S_3$ polymer/graphene hybrids as metal-free catalysts for selective photocatalytic oxidation of benzylic alcohols under visible light. ACS Catal. 4, 3302–3306.
Xu, J., Chen, Z., Zhang, H., Lin, G., Lin, H., Wang, X., Long, J., 2017. $Cd_3(C_3N_3S_3)_2$ coordination polymer/graphene nanoarchitectures for enhanced photocatalytic H_2O_2 production under visible light. Sci. Bull. 62, 610–618.
Xu, J., Fujitsuka, M., Kim, S., Wang, Z., Majima, T., 2019. Unprecedented effect of CO_2 calcination atmosphere on photocatalytic H_2 production activity from water using g-C_3N_4 synthesized from triazole polymerization. Appl. Catal. B: Environ. 241, 141–148.
Yan, W., Yu, Y., Zou, H., Wang, X., Li, P., Gao, W., Wang, J., Wu, S., Ding, K., 2018. Promoted Photocatalytic Hydrogen Evolution by Molecular Ring-Substituting Doping and Regulation of Charge Carrier Migration in Graphitic Carbon Nitride. Solar RRL 2, 1800058.
Yang, P., Ou, H., Fang, Y., Wang, X., 2017. A facile steam reforming strategy to delaminate layered carbon nitride semiconductors for photoredox catalysis. Angew. Chem. Int. Ed. 56, 3992–3996.
Yang, Y., Zhang, C., Huang, D., Zeng, G., Huang, J., Lai, C., Zhou, C., Wang, W., Guo, H., Xue, W., Deng, R., Cheng, M., Xiong, W., 2019. Boron nitride quantum dots decorated ultrathin porous g-C_3N_4: intensified exciton dissociation and charge transfer for promoting visible-light-driven molecular oxygen activation. Appl. Catal. B: Environ. 245, 87–99.
Ye, S., Zeng, G., Wu, H., Zhang, C., Liang, J., Dai, J., Liu, Z., Xiong, W., Wan, J., Xu, P., 2017. Co-occurrence and interactions of pollutants, and their impacts on soil remediation-A review. Crit. Rev. Env. Sci. Tec. 47, 1528–1553.
Ye, S., Yan, M., Tan, X., Liang, J., Zeng, G., Wu, H., Song, B., Zhou, C., Yang, Y., Wang, H., 2019. Facile assembled biochar-based nanocomposite with improved graphitization for efficient photocatalytic activity driven by visible light. Appl. Catal. B: Environ. 250, 78–88.
Yi, H., Yan, M., Huang, D., Zeng, G., Lai, C., Li, M., Huo, X., Qin, L., Liu, S., Liu, X., Li, B., Wang, H., Shen, M., Fu, Y., Guo, X., 2019. Synergistic effect of artificial enzyme and 2D nano-structured Bi2WO6 for eco-friendly and efficient biomimetic photocatalysis. Appl. Catal. B: Environ. 250, 52–62.
Yu, Y., Yan, W., Gao, W., Li, P., Wang, X., Wu, S., Song, W., Ding, K., 2017. Aromatic ring substituted g-C3N4 for enhanced photocatalytic hydrogen evolution. J. Mater. Chem. A 5, 17199–17203.
Yu, Y., Yan, W., Wang, X., Li, P., Gao, W., Zou, H., Wu, S., Ding, K., 2018. Surface engineering for extremely enhanced charge separation and photocatalytic hydrogen evolution on g-C_3N_4. Adv. Mater. 30, 1705060.
Yuan, J., Liu, X., Tang, Y., Zeng, Y., Wang, L., Zhang, S., Cai, T., Liu, Y., Luo, S., Pei, Y., Liu, C., 2018. Positioning cyanamide defects in g-C_3N_4: Engineering energy levels and active sites for superior photocatalytic hydrogen evolution. Appl. Catal. B: Environ. 237, 24–31.
Zhang, G., Wang, X., 2013. A facile synthesis of covalent carbon nitride photocatalysts by Co-polymerization of urea and phenylurea for hydrogen evolution. J. Catal. 307, 246–253.
Zhang, M., Wang, X., 2014. Two dimensional conjugated polymers with enhanced optical absorption and charge separation for photocatalytic hydrogen evolution. Energy Environ. Sci. 7, 1902.
Zhang, S., Wang, L., Liu, C., Luo, J., Crittenden, J., Liu, X., Cai, T., Yuan, J., Pei, Y., Liu, Y., 2017. Photocatalytic wastewater purification with simultaneous hydrogen production using MoS2 QD-decorated hierarchical assembly of ZnIn2S4 on reduced graphene oxide photocatalyst. Water Res. 121, 11–19.
Zhang, L., Zhang, J., Zeng, G., Dong, H., Chen, Y., Huang, C., Zhu, Y., Xu, R., Cheng, Y., Hou, K., 2018. Multivariate relationships between microbial communities and environmental variables during co-composting of sewage sludge and agricultural waste in the presence of PVP-AgNPs. Bioresour. Technol. 261, 10–18.
Zhang, J., Wang, H., Yuan, X., Zeng, G., Tu, W., Wang, S., 2019. Tailored indium sulfide-based materials for solar-energy conversion and utilization. J. Photochem. Photobiol. C Photochem. Rev. 38, 1–26.
Zheng, Y., Lin, L., Wang, B., Wang, X., 2015. Graphitic carbon nitride polymers toward sustainable photoredox catalysis. Angew. Chem. Int. Ed. 54, 12868–12884.
Zheng, Y., Yu, Z., Ou, H., Asiri, A.M., Chen, Y., Wang, X., 2018. Black phosphorus and polymeric carbon nitride heterostructure for photoinduced molecular oxygen activation. Adv. Funct. Mater. 28, 1705407.
Zhou, C., Lai, C., Xu, P., Zeng, G., Huang, D., Li, Z., Zhang, C., Cheng, M., Hu, L., Wan, J., Chen, F., Xiong, W., Deng, R., 2018a. Rational Design of Carbon-Doped Carbon Nitride/$Bi_{12}O_{17}Cl_2$Composites: A Promising Candidate Photocatalyst for Boosting Visible-Light-Driven Photocatalytic Degradation of Tetracycline. ACS Sustain. Chem. Eng. 6, 6941–6949.
Zhou, C., Lai, C., Xu, P., Zeng, G., Huang, D., Zhang, C., Cheng, M., Hu, L., Wan, J., Liu, Y., Xiong, W., Deng, Y., Wen, M., 2018b. In Situ Grown AgI/$Bi_{12}O_{17}Cl_2$ Heterojunction Photocatalysts for Visible Light Degradation of Sulfamethazine: Efficiency, Pathway, and Mechanism. ACS Sustain. Chem. Eng. 6, 4174–4184.
Zhou, M., Wang, S., Yang, P., Huang, C., Wang, X., 2018c. Boron Carbon Nitride Semiconductors Decorated with CdS Nanoparticles for Photocatalytic Reduction of CO_2. ACS Catal. 8, 4928–4936.
Zhou, Z., Zhang, Y., Shen, Y., Liu, S., Zhang, Y., 2018d. Molecular engineering of polymeric carbon nitride: advancing applications from photocatalysis to biosensing and more. Chem. Soc. Rev. 47, 2298–2321.
Zhou, C., Lai, C., Huang, D., Zeng, G., Zhang, C., Cheng, M., Hu, L., Wan, J., Xiong, W., Wen, M., Wen, X., Qin, L., 2018e. Highly porous carbon nitride by supramolecular preassembly of monomers for photocatalytic removal of sulfamethazine under visible light driven. Appl. Catal. B: Environ. 220, 202–210.
Zhou, C., Xu, P., Lai, C., Zhang, C., Zeng, G., Huang, D., Cheng, M., Hu, L., Xiong, W., Wen, X., Qin, L., Yuan, J., Wang, W., 2019a. Rational design of graphic carbon nitride copolymers by molecular doping for visible-light-driven degradation of aqueous sulfamethazine and hydrogen evolution. Chem. Eng. J. 359, 186–196.
Zhou, C., Huang, D., Xu, P., Zeng, G., Huang, J., Shi, T., Lai, C., Zhang, C., Cheng, M., Lu, Y., Duan, A., Xiong, W., Zhou, M., 2019b. Efficient visible light driven degradation of sulfamethazine and tetracycline by salicylic acid modified polymeric carbon nitride via charge transfer. Chem. Eng. J. 370, 1077–1086.
Zhou, C., Zeng, Z., Zeng, G., Huang, D., Xiao, R., Cheng, M., Zhang, C., Xiong, W., Lai, C., Yang, Y., Wang, W., Yi, H., Li, B., 2019c. Visible-light-driven photocatalytic degradation of sulfamethazine by surface engineering of carbon nitride : Properties, degradation pathway and mechanisms. J. Hazard. Mater., 120815.